Journal of Structural Geology, Vol. 10, No. 7, pp. 685 to 699, 1988
Printed in Great Britain

0191-8141/88 $03.00 + 0.00

Using joint interactions to estimate paleostress ratios

R. DYER*

Stanford Rock Physics Group, Department of Geophysics, Stanford University, Stanford, CA 94305, U.S.A.

(*Received* 9 *June* 1986; *accepted in revised form* 20 *April* 1988)

Abstract—Because they grow perpendicular to a minimum principal stress (σ_3), joints are paleostress markers. Younger joints may show a systematic change in orientation as they approach older, throughgoing, joints. This change in orientation reflects a change in the stress field in which the younger joint set is growing. Analytical solutions for the stress field around a single joint subject to a combination of opening (Mode I) and anti-plane shear (Mode III) loadings are given. The sense of rotation and change in magnitude of principal stresses near an existing joint are functions of the orientation and ratio of magnitudes of the far-field stresses and the coefficient of friction across the joint.

Assuming that a later, non-parallel joint nucleates distant from, and grows toward, the throughgoing joint, the stress field in which it is growing will be systematically rotated and changed by the presence of the throughgoing joint. The effect of interaction between the older and younger joints is ignored in the analysis. The systematic change in orientation of the later joint reflects the change in principal stresses near the throughgoing joint, and can be used to place approximate limits on the ratio of the far-field horizontal stresses.

Zoned joints are individual, subparallel en échelon joints which are confined to a narrow zone, separated from adjacent zones by a characteristic distance, and confined to a single lithologic interval. A joint zone can be modeled as a single, infinitely long joint with a characteristic height.

Comparison of analytic stress field solutions with field examples of interacting zoned joints in Arches National Park, Utah, suggest that a curving-parallel geometry of younger joints is indicative of a stress field in which $-3 < \sigma_2^\infty/\sigma_3^\infty < -1/3$. A curving-perpendicular geometry of younger zones is compatible with principal stress ratios of $-1/3 < \sigma_2^\infty/\sigma_3^\infty < 1$.

Table of symbols

J_i^k	the ith set of zoned joints in domain k
c	crack half-length (or half-height)
X, Y, Z	axes of Cartesian co-ordinate system
x, y, z	Cartesian co-ordinates
ζ	angle between σ_2^∞ and Z-axis (Fig. 7)
ψ	angle between σ_2 and Z-axis
$r_m, \theta_m; r_1, \theta_1; r_2, \theta_2$	polar co-ordinates from crack mid-point and tips (see Fig. 14)
P_i	uniform fluid pressure within the crack
P	uniform fluid pressure throughout the body
$\sigma_1^\infty, \sigma_2^\infty, \sigma_3^\infty$	far-field principal stresses
$\sigma_{xx}^\infty, \sigma_{yy}^\infty, \sigma_{zz}^\infty, \sigma_{yz}^\infty$	resolved far-field stresses on plane of crack
$\sigma_1, \sigma_2, \sigma_3$	local principal stresses
$\sigma_{xx}, \sigma_{yy}, \sigma_{zz}, \sigma_{xy}, \sigma_{xz}, \sigma_{yz}$	stresses resolved to Cartesian co-ordinate system
$\bar{\sigma}_{zz}^\infty$	far-field uniform stress in Z-direction
σ_{zz}^I	induced stress in Z-direction to satisfy plane strain
K_i	stress intensity in ith mode of deformation
K_i^C	fracture toughness in ith mode of deformation
C^0	coefficient of sliding friction
S	shear stress ratio
ν	Poisson's ratio

INTRODUCTION

ENGELDER & Geiser (1980) concluded from field studies on the Appalachian Plateau that regional systematic joints reflect the principal directions of the regional stress field which gave rise to the joints. Each set of joints is interpreted to represent a distinct episode of jointing and an associated stress field. They concluded (Engelder & Geiser 1980, p. 6333) that joints are extensional fractures formed perpendicular to σ_3 and inferred that net tensile stresses were present during jointing. Superposition of multiple sets reflects a change in the orientation of regional stresses over time.

There is a consistent interactive geometry between different sets of systematic joints in some areas. This geometry allows the relative ages of the systematic sets to be determined. Younger joints terminate against the free surface represented by the wall of an older joint, unless the walls of the older joints were effectively cemented together (Wheeler & Holland 1981, p. 397). Additionally, younger joints may abruptly curve near an older joint, resulting in a 'hook' geometry (Kulander *et al.* 1979). Younger joints may also curve into parallelism with the older joint (Dyer 1983). These geometries are herein termed curving-perpendicular and curving-parallel geometries.

Elastic solutions for the stress field about a crack in an otherwise homogeneous body predict a perturbation of the stress field in the vicinity of the crack. The region of perturbed stresses is dependent on a characteristic length, the crack length or height. A change in orientation of the principal stresses in this perturbed zone should be reflected by a change in orientation of any younger crack which grows into the perturbed zone around the older crack.

Expanding on the terminology of Hodgson (1961), zoned joints are a type of systematic joint in which all

*Present address: Department of Geological Sciences, University of Texas at El Paso, El Paso, TX 79968, U.S.A.

joints of a given geometric set are confined to a narrow zone, generally perpendicular to bedding. Zones of a given set display a characteristic interzone spacing over a large region. Joints within a given zone display no consistent en échelon pattern in either map or cross-section view. The relatively simple geometry of zoned joints justifies a comparison between observed interaction geometries between sets of zoned joints and analytical solutions to the stress field about a single, idealized joint.

This paper presents observations on zoned joints from Arches National Park, Utah, U.S.A., and compares observed interactions to those predicted by analytical solutions to the stress field about a single, idealized joint zone.

EXAMPLES OF JOINT INTERACTIONS

Exceptional exposures of systematic joints are found on the flanks of the Salt Valley Anticline in Arches National Park, Southeastern Utah, U.S.A. The Salt Valley Anticline is the northwestern exposure of a series of en échelon salt-cored anticlines which make up the Paradox Basin region of the Colorado Plateau Province. Numerous investigators have studied the geology of this area (Dane 1935, Williams 1964, Cater 1970, Baars & Stevenson 1981, Dyer 1983, Doelling 1985). A generalized geologic map is shown in Fig. 1.

Systematic joints are well developed in several stratigraphic units on the anticline, but one unit displays exceptional exposures over an outcrop area of about 50 km^2. This unit is the Moab Member of the Entrada Sandstone. It is a sheet-like body of Jurassic eolian quartzose sandstone with a uniform thickness of 27 m and displaying large-scale cross-bedding. The Moab conformably overlies a thick (69–96 m) section of alternating planar- and cross-bedded siltstones and sandstones of the Slick Rock member of the Entrada Sandstone. The Summerville Formation conformably (?) overlies the Moab (but also see O'Sullivan 1981, and Doelling 1985 for other interpretations). The Summerville is about 12 m thick, and is composed of alternating thin beds of claystone, sandstone and limestone.

Several sets of systematic joints are developed in the Moab, with a mean strike almost parallel to the axis of the Salt Valley Anticline. Systematic jointing in the Moab Member provides classic examples of zoned joints. Due to the nature of joint zones, relative ages of joint sets can be readily determined. Detailed observation of the offset of sand dune cross-bedding in the Moab Member allows lateral shear displacement to be determined, and rules out a shearing origin for the joints.

The age of the successive jointing episodes and the relevant boundary conditions (namely the depth of burial and the influence of fluid pressure) present during each episode are poorly constrained. None of the sets of systematic joints shows any change in orientation near present erosional features such as canyon walls. This suggests that all systematic joint sets formed under an unknown thickness of overburden prior to the most recent erosional event. Conversely, analysis of the relationship between curvature of the Moab sheet and the orientation of systematic joints indicates that the youngest systematic joints are almost perpendicular to the local maximum convex-upward curvature of the Moab sheet (Dyer 1979). Superimposed systematic joint sets in the Moab are compatible with a response to repeated flexing of the brittle Moab sheet due to the movement of underlying salt. In this model, the youngest joints formed in response to local tensile stresses due to passive bending of the Moab sheet over mobile salt. The latest phase of collapse of the Salt Valley Anticline is known to have started not more than 600,000 years ago (Dyer *et al.* 1983). It is doubtful that more than 1 km of overlying rock has been removed by erosion in the intervening 600,000 years.

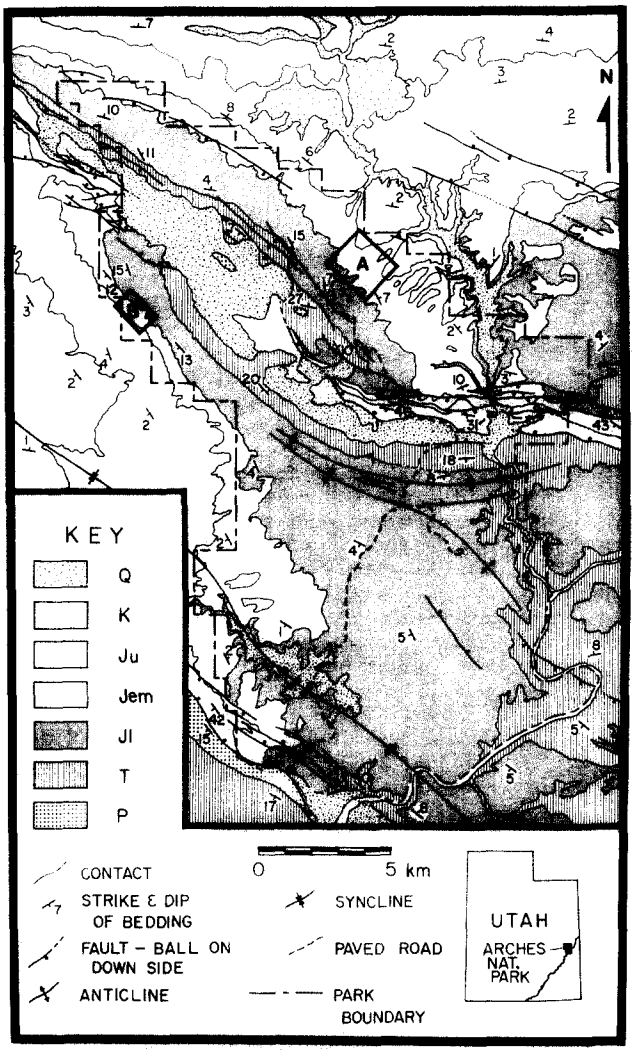

Fig. 1. Generalized geologic map of Arches National Park and vicinity (after Doelling 1985). Rectangles A and B correspond to joint Domains A and B (Figs. 2a and 3a). Map units are: Q = Quaternary alluvium and colluvium; K = Cretaceous marine shale and minor sandstone; Ju = Upper Jurassic continental sandstones and shale; Jem = Jurassic Moab Member of Entrada Sandstone (eolian sandstone); Jl = Lower Jurassic eolian and fluvial sandstone; T = Triassic continental and marginal marine sandstone; P = Pennsylvanian and Permian evaporites, limestone and sandstone.

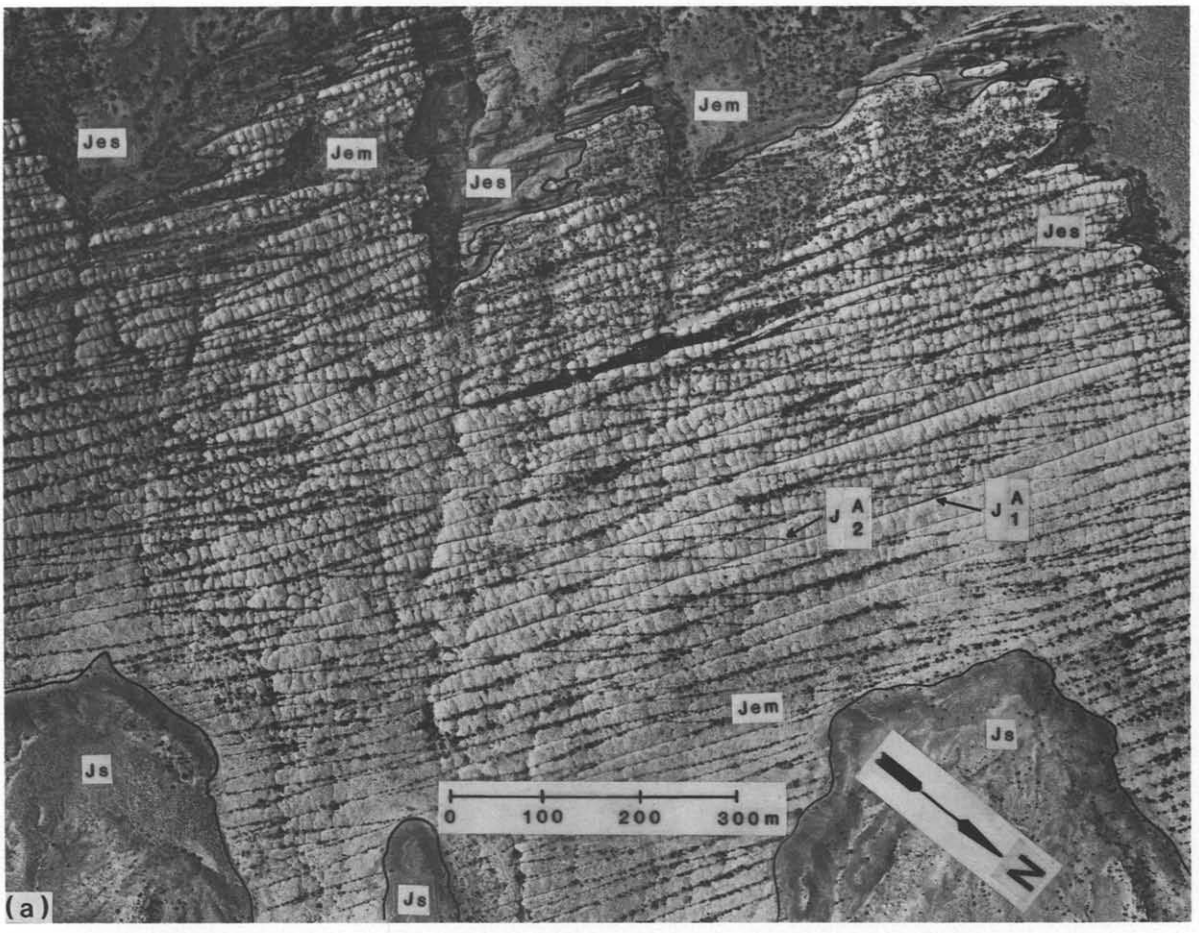

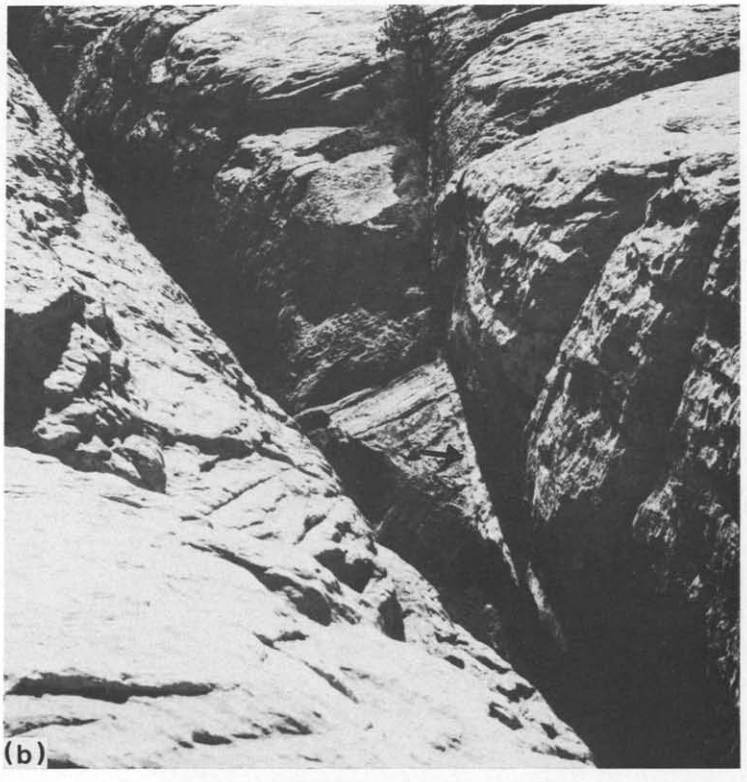

Fig. 2. (a) Aerial view of part of Domain A. Enlargement is portion of frame GS-WI 26-101, U.S. Geological Survey aerial mapping photography. Jes = Slick Rock Member; Jem = Moab Member; Js = Summerville Formation. Characteristics of J_1^A and J_2^A explained in text. Note that J_2^A nowhere crosses J_1^A. Sigmoidal shape of J_2^A is apparent near annotations, and is best seen when page is tilted and viewed along J_1^A. (b) View looking down J_2^A zone. Juniper tree growing in J_2^A is about 2 m tall. J_1^A trends from upper left to lower right. Note how near-planar joints in J_2^A (at arrow) systematically change orientation as J_2^A approaches J_1^A.

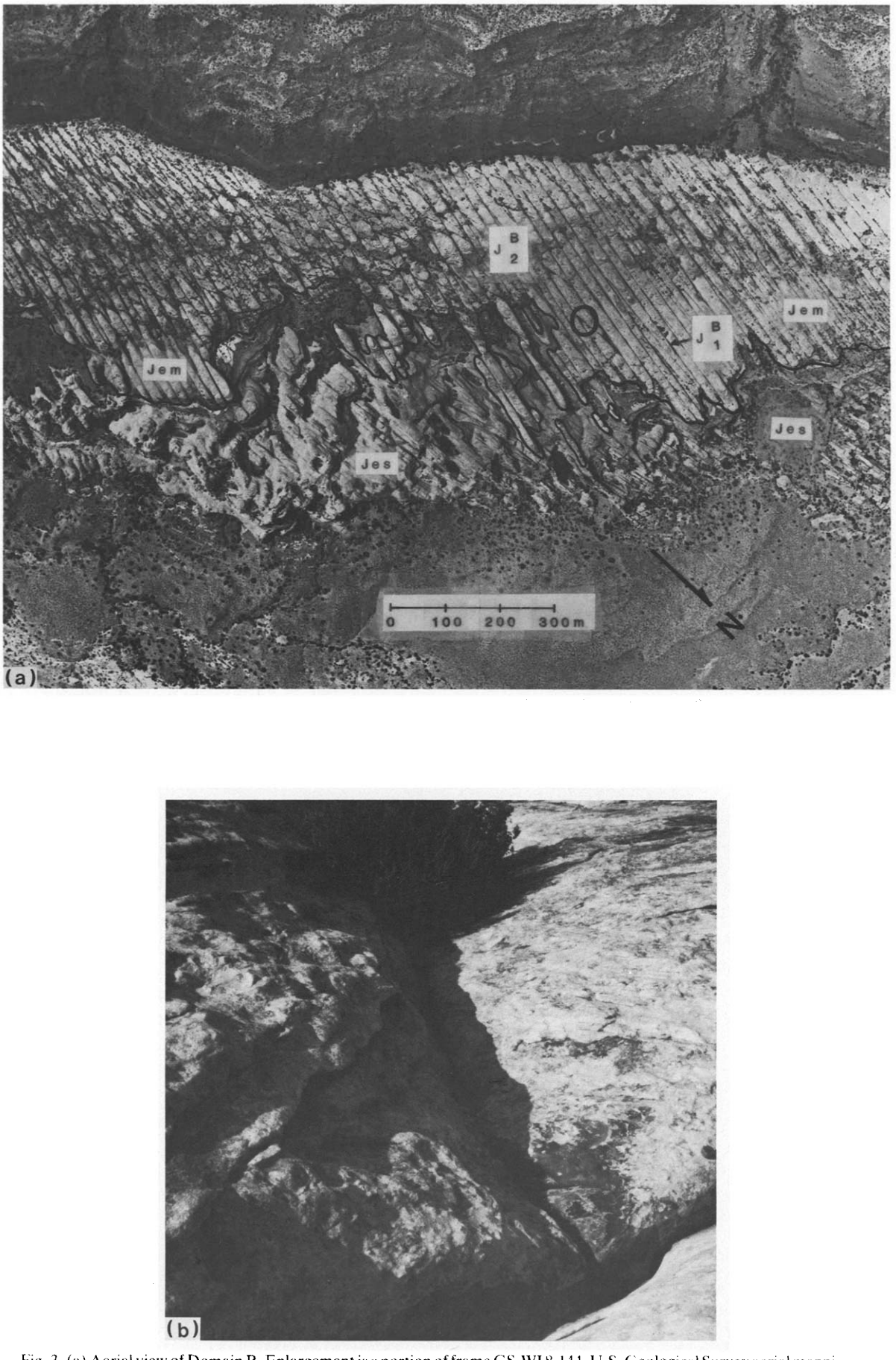

Fig. 3. (a) Aerial view of Domain B. Enlargement is a portion of frame GS-WI 8-144, U.S Geological Survey aerial mapping photography. Jes = Slick Rock Member; Jem = Moab Member; J_1^B and J_2^B explained in text. Circle indicates location of (b). Note jointing in underlying Slick Rock. (b) View down a J_2^B zone. J_1^B trends from lower left to center right. Brunton compass in center right for scale. Note that J_2^B intersects J_1^B at nearly a right angle, and is terminated by J_1^B.

Observations

Figures 2 and 3 show superimposed sets of zoned systematic joints which are developed in the Moab. Based on widespread geometric characteristics, two distinct domains of zoned joints are differentiated.

In Domain A, the oldest joint zones are throughgoing features (J_1^A of Fig. 2a) which display 2–6 cm of right-lateral shear displacement. Younger joint zones are collectively referred to as J_2^A. The dihedral angle between the mean attitudes of J_1^A and J_2^A ranges from 6 to 23° with a distinct maximum at 10°. Lateral displacement on J_2^A zones ranges from zero to 2 cm, with only right-lateral displacement noted. J_2^A zones with more easterly strikes display the least shear displacement and are interpreted to be the youngest joint zones in Domain A. J_2^A zones do *not* cut, nor do they intersect, joints of the first set. J_2^A zones are entirely bound between two adjacent zones of J_1^A. J_2^A zones do not appear to nucleate along J_1^A zones, but rather in the central region between J_1^A zones. Traces of J_2^A zones are linear in the central region between flanking J_1^A zones, but begin to curve into parallelism with J_1^A zones at a distance typically of about 5 m. The closer J_2^A comes to J_1^A, the more pronounced the curvature, with J_2^A finally paralleling J_1^A some tens of centimeters away (Fig. 2b). This *curving-parallel* geometry of J_2^A produces the sigmoidal form apparent in Fig. 2.

The oldest joint zones of Domain B are also throughgoing, planar features (J_1^B of Fig. 3a). J_1^B zones uniformly display left-lateral displacement of 1–6 cm. Later generations of joint zones in this region are collectively designated J_2^B. The strike of J_2^B varies considerably, from N10°E to N39°W, giving J_1^B/J_2^B dihedral angles of 2–51°. As was the case in Domain A, J_2^B joint zones do not cut across J_1^B zones, but are bound by J_1^B. J_2^B zones show a consistent curving-perpendicular geometry. The J_2^B zones consistently curve abruptly *toward* the throughgoing J_1^B zones, with J_2^B intersecting and terminating in a J_1^B zone at almost a right angle (Fig. 3b). The change in strike of J_2^B occurs very abruptly, typically about 1–2 m from the J_1^B zone. Lateral offset on J_2^B varies from less than 1 mm to about 1.2 cm, with all observed offset being left-lateral. J_2^B joints with more westerly strikes show the least offset and are interpreted to be the youngest systematic joints in Domain B.

Discussion

The age relationships in Domains A and B are unambiguous. Within each domain, all J_1 zones clearly predate all J_2 zones. These two sets of zoned joints are *not* synchronous, conjugate joints. The youngest sets of systematic joints, J_2, generally show no shear displacement, only a dilational opening. Zoned joints of J_2 were formed as extensional fractures. Collectively, they appear to have formed during an episode of jointing in which the causative stress field had rotated relative to that which caused J_1 (Fig. 4).

Although the throughgoing zones of J_1 may display small horizontal shear displacements, they are also inferred to have originated as extensional fractures. Support for this interpretation is mostly circumstantial: the presence of only one set of sub-parallel joints and the lack of a regular en échelon geometry argue against a shearing origin in which conjugate sets might be expected to form; while the uniform sense of shear displacement observed on J_1 is compatible with later shear displacement due to a rotational stress field in which the extensional joints of J_2 were growing.

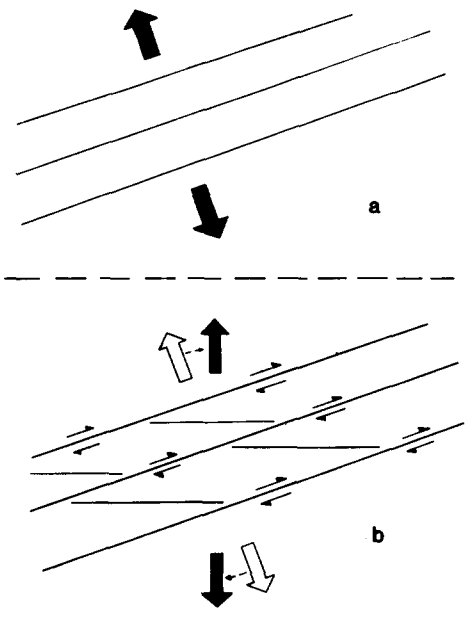

Fig. 4. (a) Throughgoing zoned joint set forms perpendicular to regional least principal stress (arrows). (b) Over time, rotation of stress field leads to resolved shear stresses on the throughgoing set of zoned joints, which in turn causes shear displacement on the oldest set. Younger zoned joints growing in this rotated stress field nucleate in the region between the throughgoing zones, perpendicular to the new direction of σ_3 (heavy arrows). Compare with Figs. 2(a) and 3(a).

The uniform manner in which younger joint zones change their attitude throughout a domain (curving-parallel in Domain A and curving-perpendicular in Domain B) suggests that the presence of the older joint set has a locally strong influence on the growth of the later set. In map view, the later (J_2) zones display a sigmoidal shape, similar to that seen in asymmetric tension gashes (Roering 1968, Ramsay & Graham 1970, Durney & Ramsay 1973). A standard explanation of such tension gashes is that they represent the localized, progressive rotation by simple shear of an originally planar crack which continued to grow during the shearing deformation, while the causative stress field remains fixed in orientation (Ramsay 1967, pp. 88–91). The resolved shear gives rise to a progressive rotation of the inner core of the tension gash, while later increments of crack growth are oriented perpendicular to the far-field least principal stress direction. Such a mechanism requires material rotation in a fixed stress field. This mechanism has been used to account for the 'anomalous' curvature commonly noted in en échelon fractures wherein the "ends of the gashes curve toward the direc-

tion from which movement occurred" (Shainin 1950, p. 516).

Simple shear and progressive material rotation can be ruled out as the cause of the sigmoidal form of the younger joint zones in Arches. Such progressive rotation would require meters to tens of meters of lateral offset along the J_1 zones, while field observations rule out more than 10 cm of lateral offset and any significant penetrative strain. Estimates of shear displacement arrived at by examining the deflected angle of the sigmoidal form have no relation to the true lateral offset observed on the throughgoing joint set J_1.

An alternate hypothesis is that the throughgoing joint zone, J_1, locally perturbed the stress field in which a younger joint set (J_2) was growing. This perturbation caused rotations of the orientation of the principal stresses and also resulted in a change of the magnitudes of the principal stresses. The perturbing effect was apparently strongest closest to the throughgoing joint zone. Thus, the sigmoidal form would not have arisen from a material rotation in a fixed stress field, but from a local rotation of the stress field due to an inhomogeneity in the rock layer. A pre-existing joint zone could certainly have provided such an inhomogeneity.

In Arches, the curving-perpendicular geometry of younger joint zones in Domain B is associated with left-lateral displacement across the older throughgoing zones. Conversely, the curving-parallel geometry of younger joint zones in Domain A is associated with right-lateral displacement across the throughgoing zones (Fig. 5). It is tempting to associate curving-parallel geometries with right-lateral displacements and the curving-perpendicular geometries with left-lateral displacements along the throughgoing zones. This association, however, is not true in general. It is possible for a younger joint zone to develop either (and perhaps both) of the sigmoidal geometries in a given region, regardless of the resolved sense of shear and displacement across the older, throughgoing zone.

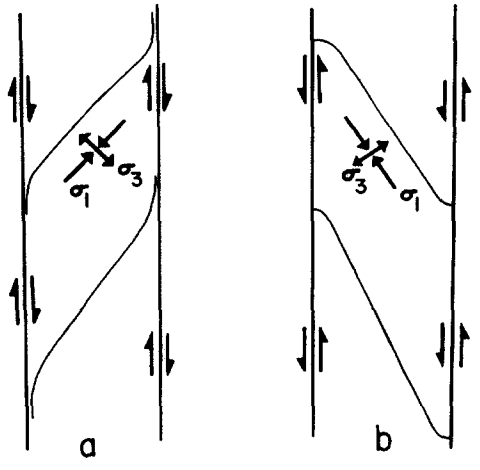

Fig. 5. Cartoon map of (a) Domain A and (b) Domain B, showing: the observed sigmoidal geometry of younger joints; the observed sense of shear displacement on older, throughgoing joint zones, and the inferred orientation of the principal stresses in the mid-region between the throughgoing zones during the latest phase of jointing.

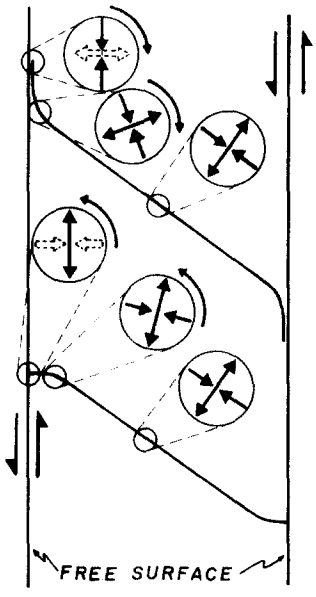

Fig. 6. Cartoon map view of the two ways in which the state of stress may rotate to accommodate a free surface at a throughgoing joint zone. Orientation and magnitude of principal stresses in mid-region between throughgoing zones approximates the remote stresses. One principal stress is assumed to be vertical. Younger joint zone grows outward from the mid-region between older, throughgoing joints, with each growth increment perpendicular to the local minimum principal stress (σ_3). Sigmoidal geometry develops due to rotation of principal stresses near the free surface. Sense of rotation is mainly a function of the ratio of the remote stresses, and hence will remain uniform over a relatively large area during a given jointing episode. This leads to the occurrence of a single sigmoidal geometry over this area, or domain.

In general, the throughgoing zones may be considered as free surfaces, which requires that at the throughgoing zones, one of the principal stresses be perpendicular to the joint face and have zero magnitude. Examination of the state of stress in the region between two throughgoing zones indicates that this requires a rotation in space of the principal stresses, and a change in magnitude of at least one of the principal stresses (Fig. 6). The rotation of the principal stresses may either be clockwise (Fig. 6, top) or counterclockwise (Fig. 6, bottom).

JOINTS AS PALEOSTRESS INDICATORS

Joints record an episode of brittle fracture in rock. Field evidence indicates that all of the zoned systematic joints in Arches originated as extensional fractures. As noted by Griggs & Handin (1960, p. 348), extension fractures form perpendicular to the direction of σ_3. Tensile fractures are a subset of extension fractures which form due to a tensile σ_3 (more correctly, when $\sigma_3 - P < 0$, where P is a uniform fluid pressure within the crack). There is a considerable body of theoretical and experimental evidence to support this geometric relation between the orientation of the extension fracture and the orientation of σ_3 (Hubbert & Willis 1957, Odé 1957, Griggs & Handin 1960, pp. 350–351, Kehle 1964, Hoek & Bieniawski 1965, Secor 1965, 1969, Peng & Ortiz 1973, Zoback & Pollard 1978). The zoned joints of

Arches, then, provide a paleostress map of the elastic stress field at the time of jointing. The consistent change in orientation of younger joint zones near older, throughgoing zones is interpreted as a local change in the stress field due to the presence of the throughgoing zone.

Solutions for the elastic stress field about an idealized single zone of joints are presented in the following pages. Assumptions about loading conditions allow a considerable simplification of the solutions. Maps are presented of the stress field about a single joint zone for a variety of loading conditions. These stress maps are interpreted in terms of the geometry that a younger joint set might develop if growing in this stress field. The interpretations involve rather restrictive assumptions. These assumptions are: (1) a tensile minimum principal stress (σ_3) is required for joint growth; (2) orientation of the tip of the growing joint is perpendicular to the local σ_3; and, (3) there is no interaction between the throughgoing joint and the growing joint. Comparisons are made with the systematic change in orientation observed in the younger zoned joints in Domains A and B. No explicit provision is made in this analysis for an internal fluid pressure, P, within the joint. If such a fluid pressure were present, assumption (1) can be more rigorously stated as: joint growth requires that $(\sigma_3 - P) < 0$. If the fluid pressure is uniform and unchanging in space and time the analysis presented below can be recast in terms of effective principal stresses without changing the analysis or results. The generalized solutions of the Appendix allow for the addition of a uniform 'excess' internal fluid pressure (an overpressure) within the joint. Unfortunately, there is no evidence from which to determine or estimate the magnitude or spatial variation of P during the jointing episodes in Arches, so this potentially important factor is ignored in the following analyses.

An elastic analysis indicates that the presence of a crack in an otherwise homogeneous, infinite isotropic body will locally perturb the stress field in the vicinity of the crack, leading to a local rotation and change in magnitude of the principal stresses. Although the criteria for the direction of growth of a later crack in such an inhomogeneous stress field is not certain, most theories (summarized in Bergkvist & Guex 1979) point toward the same end result: the younger crack will grow in a direction to align itself with the direction of the local principal stresses, that is the direction of crack growth will be such that it minimizes the resolved shear on the propagating crack tip. Using this criterion, we might expect a second crack growing in the perturbed stress field due to the presence of the throughgoing crack to follow the trace of the rotating principal stresses in the perturbed zone. Such a criterion ignores the interaction between cracks (Segall & Pollard 1980) and the attraction effect which a free surface has on the growing crack (Pollard & Holzhausen 1979). The complete problem, accounting for interactions between the two cracks, is not readily solvable by analytic means.

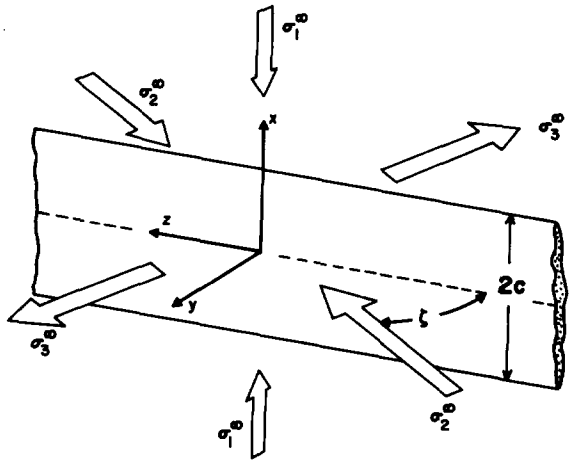

Fig. 7. Idealization of a joint zone as a single, infinitely long crack of height $2c$. The crack is subjected to far-field stresses in the horizontal plane (σ_3^∞ and σ_2^∞). σ_1^∞ is vertical and colinear with the X-axis.

STRESS FIELD ABOUT OLDER JOINT ZONE

Within a given domain, non-parallel generations of zoned joints display one of two characteristic interactions: (A) the younger joint zone curves into parallelism with the older joint zone; and (B) the younger joint zone intersects the older zone at nearly a right angle. Some insight into the physical basis for this behavior may be gained from an elastic analysis of local stress perturbations about the older, throughgoing zone.

The older joint zone may be considered mechanically equivalent to a single, infinitely long crack which has a characteristic height of $2c$ (Fig. 7), and which is embedded in an infinite, isotropic, homogeneous elastic body. The crack is subjected to mixed Mode I (opening mode) and Mode III (antiplane shear) loading.

The loading arises from far-field principal stresses σ_1^∞, σ_2^∞ and σ_3^∞. We use the sign convention that positive stresses are compressive and negative stresses are tensile. The field evidence requires that $(\sigma_3^\infty - P) < 0$ and that σ_3^∞ lie in the horizontal (Y–Z) plane. Because no estimates of the value of P are available, we assume that $P = 0$, which requires that σ_3^∞ be tensile. We assume that σ_1^∞ is vertical (colinear with the X-axis) and compressive. σ_2^∞ lies in the Y–Z (horizontal) plane and may be either tensile or compressive. We will examine the changes in the stress field about the crack under various ratios of $\sigma_2^\infty/\sigma_3^\infty$.

Resolved stresses on the crack

The far-field principal stresses, resolved into normal and shear components with respect to the crack face give:

$$\sigma_{yy}^\infty = \left[\frac{\sigma_2^\infty + \sigma_3^\infty}{2}\right] - \left[\left(\frac{\sigma_2^\infty - \sigma_3^\infty}{2}\right)\cos\left[2(90 - \zeta)\right]\right] \quad (1)$$

$$\sigma_{zz}^\infty = \left[\frac{\sigma_2^\infty + \sigma_3^\infty}{2}\right] + \left[\left(\frac{\sigma_2^\infty - \sigma_3^\infty}{2}\right)\cos\left[2(90 - \zeta)\right]\right] \quad (2)$$

$$\sigma^{\infty}_{yz} = \left(\frac{\sigma^{\infty}_2 - \sigma^{\infty}_3}{2}\right) \sin\,[2(90 - \zeta)] \tag{3}$$

$$\sigma^{\infty}_{xx} = \sigma^{\infty}_1, \tag{4}$$

where ζ is the angle between σ^{∞}_2 and the Z-axis (Fig. 7).

Solving for the stress field

The general loading is shown in Fig. 8. Because of the presence of the crack (zoned joint), local variations in the stress field may occur. These variations will result in changes in the magnitude and orientation of the principal stresses. Solution of the problem must be independent of z, so the problem reduces to a superposition of two-dimensional problems in the X–Y plane and a uniform stress on the Z-axis (Fig. 8b or c, d & e). Details of the solution for the perturbed stresses σ_{xx}, σ_{yy}, σ_{xy} and σ_{yz} are given in the Appendix. The stress along the Z-axis, σ_{zz}, is the sum of a far-field uniform stress, $\bar{\sigma}^{\infty}_{zz}$, and an induced stress required to satisfy the plane strain geometry of our two-dimensional solutions, σ^{I}_{zz} (Fig. 8b or c, & e).

$$\sigma_{zz} = \bar{\sigma}^{\infty}_{zz} + \sigma^{\mathrm{I}}_{zz}, \tag{5}$$

where $\sigma^{\mathrm{I}}_{zz} = \nu(\sigma_{xx} + \sigma_{yy})$ and ν is Poisson's ratio. A typical value of ν for sandstones is about 0.1 (Birch 1966, p. 167). We will assume throughout that $\nu = 0.1$.

Far from the crack we require that

$$\begin{aligned}\sigma^{\infty}_{zz} &= \bar{\sigma}^{\infty}_{zz} + \sigma^{\mathrm{I}}_{zz} \\ &= \bar{\sigma}^{\infty}_{zz} + \nu(\sigma^{\infty}_{xx} + \sigma^{\infty}_{yy}) \\ \text{so } \bar{\sigma}^{\infty}_{zz} &= \sigma^{\infty}_{zz} - \nu(\sigma^{\infty}_{xx} + \sigma^{\infty}_{yy}).\end{aligned} \tag{6}$$

If we limit our investigation to the plane $x = 0$, then the only rotation of principal stresses will be about the X-axis. Once the stresses σ_{yy}, σ_{zz} and σ_{yz} are found at a point, the orientation and magnitude of the principal stresses, σ_2 and σ_3, at that point can be found from a simple Mohr circle construction.

We limit our investigation to the plane $x = 0$ because of the great simplification in the analysis which results. Off the $x = 0$ plane, σ_{xy} and σ_{xz} shear stresses will exist which will tend to rotate the principal stresses about the Z- and Y-axes, respectively. These shearing stresses will increase near the crack tip ($y = 0, x = \pm c$).

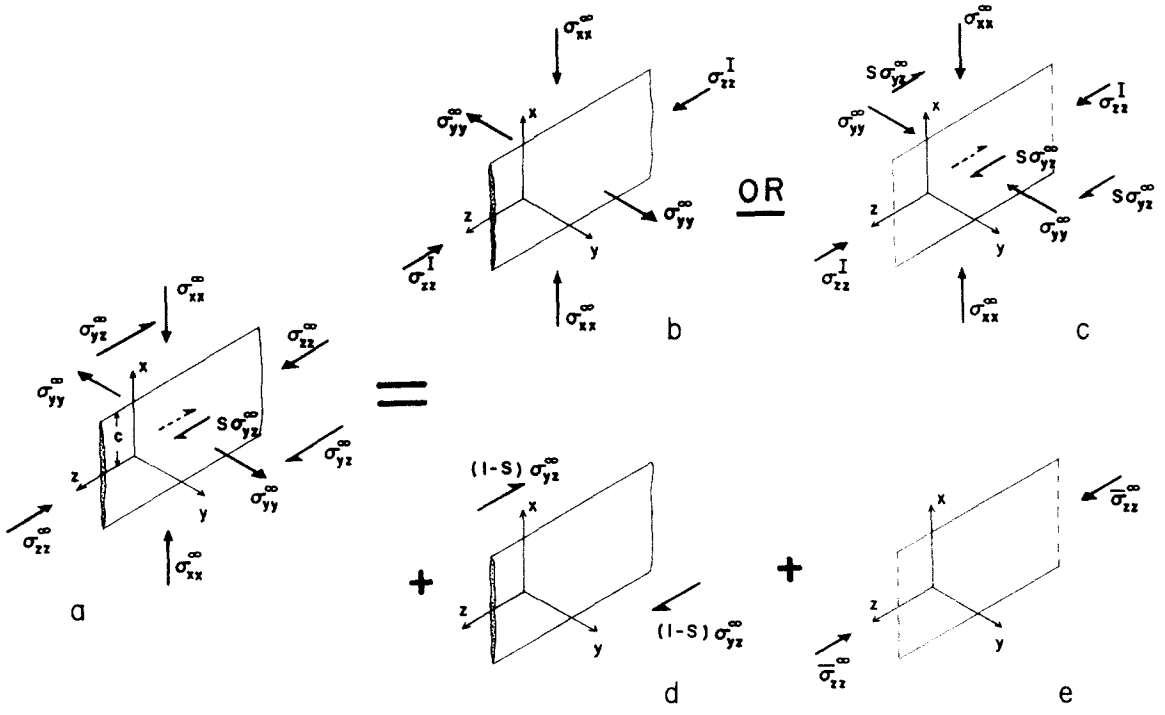

Fig. 8. (a) Resolution of principal stresses σ^{∞}_1, σ^{∞}_2 and σ^{∞}_3 into normal and shear components leads to this generalized loading on a crack which is infinitely long in the Z-direction and has a characteristic height ($= 2c$) in the X-direction. One of the principal stresses (σ^{∞}_1) is colinear with the X-axis. If σ^{∞}_{yy} is compressive, then the crack is closed and a σ^{∞}_{yz} shearing stress of magnitude $S\sigma^{\infty}_{yz}$ may exist on the crack surface. Solution of the perturbed stress field about the crack can be obtained by linear superposition of solutions to plane crack problems (b) and (d) and uniform stress states (c) and (e). Any arbitrary loading can be expressed as a combination of case (b) *or* (c), plus (d) and (e). (b) Opening mode (Mode I) crack under biaxial loading. This solution is only applicable if σ^{∞}_{yy} is tensile, which requires the crack to be open. The normal and shear stresses on the crack surface, $\sigma_{yy}(y = 0, |x| < c)$ and $\sigma_{yz}(y = 0, |x| < c)$ are zero. (c) If σ^{∞}_{yy} is compressive, then the crack is closed and σ_{yy} is continuous across the crack plane. There is no Mode I perturbation of the stress field, and uniform normal (σ^{∞}_{xx}, σ^{∞}_{yy}) and shear stresses ($S\sigma^{\infty}_{xy}$) exist throughout the body. The plane strain geometry leads to an induced σ_{zz} stress of magnitude $\sigma_{zz} = \nu[\sigma^{\infty}_{xx} + \sigma^{\infty}_{yy}]$. For any given loading, either case (b) or (c) will be applicable with each mutually exclusive of the other. (d) Another solution component is that due to pure Mode III (antiplane shear) loading. This solution satisfies the case of a far-field shear stress of magnitude $(1 - S)\,\sigma^{\infty}_{yz}$ applied to a crack whose surfaces are stress-free. If σ^{∞}_{yy} is tensile, then $S = 0$. (e) A uniform stress in the Z direction, $\bar{\sigma}^{\infty}_{zz}$ may be superimposed on the body without altering any of the other solutions.

BOUNDARY CONDITIONS

There are two general situations we wish to investigate: (1) when the throughgoing zone is an open crack, and (2) when the crack is closed and there may be frictional sliding on the crack.

Open crack ($\sigma^{\infty}_{yy} < 0$)

If the resolved far-field stress perpendicular to the crack face (σ^{∞}_{yy}) is tensile, then the crack is open, and the crack face is traction-free. The boundary conditions which must be satisfied are

$$\text{at } y = 0; \quad |x| < c; \quad \sigma_{yy} = \sigma_{yz} = 0, \tag{7}$$

$$\text{at } (x^2 + y^2)^{1/2} \to \infty; \quad \begin{cases} \sigma^{\infty}_{yy} = \sigma_{yy} \\ \sigma_{xx} = \sigma^{\infty}_{xx}. \\ \sigma_{yz} = \sigma^{\infty}_{yz} \end{cases} \tag{8}$$

This situation corresponds to a superposition of the problems illustrated in Fig. 8(b), (d) & (e). The solution is given by superposition of the plane crack Mode I and Mode III solutions (equations A9, A10 and A19 in the Appendix). On the plane $x = 0$, the non-zero stresses are

$$\sigma_{yy}(x = 0) = \sigma^{\infty}_{yy}\left[\frac{|y^3|}{(y^2 + c^2)^{3/2}}\right] \tag{9}$$

$$\sigma_{xx}(x = 0) = \sigma^{\infty}_{yy}\left[\frac{|y|(y^2 + 2c^2)}{(y^2 + c^2)^{3/2}} - 1\right] + \sigma^{\infty}_{xx} \tag{10}$$

$$\sigma_{yz}(x = 0) = \sigma^{\infty}_{yz}\left[\frac{y}{(y^2 + c^2)^{1/2}}\right] \tag{11}$$

$$\sigma_{zz}(x = 0) = \bar{\sigma}^{\infty}_{zz} + \nu(\sigma_{xx} + \sigma_{yy}). \tag{12}$$

Substituting in equations (6), (9) and (10), equation (12) becomes:

$$\sigma_{zz}(x = 0) = \bar{\sigma}^{\infty}_{zz} + \nu\left[\sigma^{\infty}_{yy}\left(\frac{2|y^3 + yc^2|}{(y^2 + c^2)^{3/2}}\right) - 2\right]. \tag{13}$$

From equations (9)–(13) the orientation and magnitude of the principal stresses σ_2 and σ_3 can be determined on the plane $x = 0$. σ_1 will be colinear with the X-axis and have the magnitude of σ_{xx} as given by equation (10). It is worth emphasizing that on the plane $x = 0$, the magnitude and orientation of σ_2 and σ_3 are independent of σ^{∞}_1.

Closed crack ($\sigma^{\infty}_{yy} > 0$)

If the resolved far-field stress perpendicular to the crack face, σ^{∞}_{yy}, is compressive, then the crack is closed and there can be no Mode I perturbation of the stress field. It is still possible for the crack to be shear-stress free. Such a situation might arise if the crack were perfectly lubricated. In general, the shear stress on the crack face will have some intermediate value between zero and σ^{∞}_{yz}. This situation corresponds to a superposition of the problems shown in Fig. 8(c), (d) & (e).

The boundary conditions for this problem are:

$$\sigma_{yy} = \sigma^{\infty}_{yy} \tag{14}$$

$$\sigma_{xx} = \sigma^{\infty}_{xx}$$

$$\text{for } y = 0, \ |x| < c; \quad \sigma_{yz} = S\sigma^{\infty}_{yz} \ (0 \leqslant S \leqslant 1) \tag{15}$$

$$\text{for } (x^2 + y^2)^{1/2} \to \infty; \quad \sigma_{yz} = \sigma^{\infty}_{yz}. \tag{16}$$

S is the shear stress ratio given by

$$S = \frac{\sigma_{yz}\,(y = 0)}{\sigma^{\infty}_{yz}}.$$

$S = 0$ corresponds to a perfectly lubricated crack, while $S = 1$ corresponds to a locked crack. If a Byerlee-type sliding friction relation is used, then on the crack face ($y = 0, |x| < c$):

$$\sigma_{yz} = C^0\sigma^{\infty}_{yy} = S\sigma^{\infty}_{yz} \tag{17}$$

$$\text{and } S = C^0\frac{\sigma^{\infty}_{yy}}{\sigma^{\infty}_{yz}},$$

where C^0 is the coefficient of sliding friction.

Solution of the boundary value problem is obtained by the superposition of two solutions corresponding to Fig. 8(c) & (d)

$$\sigma_{yz} = \sigma^{c}_{yz} + \sigma^{d}_{yz}, \tag{18}$$

where

$$\sigma^{c}_{yz} = S\sigma^{\infty}_{yz}(0 \leqslant S \leqslant 1) \tag{19}$$

is the uniform shear stress in an uncracked infinite body (Fig. 8c), and

$$\sigma^{d}_{yz} = (1 - S)\sigma^{\infty}_{yz}\left[\frac{y}{(y^2 + c^2)^{1/2}}\right] \tag{20}$$

is the shear stress at the point $(x = 0, y, z)$ due to the existence of a frictionless, infinitely long crack of height $2c$ subjected to a far-field anti-plane shear (Mode III loading) of magnitude $(1 - S)\sigma^{\infty}_{yz}$. The full Mode III solution is given in the Appendix, equation (A17). This problem is illustrated in Fig. 8(d).

Equation (18) becomes

$$\sigma_{yz}(x = 0) = \sigma^{\infty}_{yz}\left[S\left(1 - \frac{y}{(y^2 + c^2)^{1/2}}\right) + \frac{y}{(y^2 + c^2)^{1/2}}\right] \tag{21}$$

$$= \sigma^{\infty}_{yz}\left[S + (1 - S)\left(\frac{y}{(y^2 + c^2)^{1/2}}\right)\right].$$

It may easily be verified that equation (21) satisfies the boundary conditions of (15) and (16). To complete the solution, we note that:

$$\begin{aligned} &\sigma_{xx} = \sigma^{\infty}_{xx} = \sigma^{\infty}_1 \\ &\sigma_{yy} = \sigma^{\infty}_{yy} \\ &\sigma_{zz} = \bar{\sigma}^{\infty}_{zz} + \nu[\sigma^{\infty}_{xx} + \sigma^{\infty}_{yy}] = \sigma^{\infty}_{zz} \\ &\sigma_{xy} = 0. \end{aligned} \tag{22}$$

We may now solve for the principal stresses σ_2 and σ_3 on the plane $x = 0$ and determine their orientation by using the results of (21) and (22) in a standard Mohr circle construction. On $x = 0$, σ_1 will be vertical, with $\sigma_1 = \sigma^{\infty}_1$.

As with the open crack, it is worth noting that the orientation and magnitude of σ_2 and σ_3 are independent of σ_1^∞ on the plane $x = 0$.

EXAMPLES

Figures 9, 10, 12 and 13 are maps of the elastic stress field about a *single* joint under a variety of combinations of far-field stresses and degree of healing of the joint. All examples assume no excess internal fluid pressure in the joint ($P_i = 0$). All maps are of the plane $x = 0$, the near-horizontal plane perpendicular to and bisecting the joint. In all the examples, the far-field principal stresses, σ_2^∞ and σ_3^∞, lie in the Y–Z plane, and σ_2^∞ makes an angle of 30° with the joint face (the Z-axis). The positive X-axis (approximately vertical) is normal to the page. The trace of the joint falls on the Z-axis. On the plane $x = 0$, the solution is independent of the z co-ordinate. For generality, the Y-axis has been non-dimensionalized. For comparative purposes, the joint half-height [c] in the Moab Member is 13.5 m. Stresses are in arbitrary units.

If we accept the hypothesis that the local crack propagation direction is perpendicular to the local minimum principal stress, then it is tempting to use the perturbed elastic stress field to make a predictive plot of the trace of a joint which grows in the perturbed stress field. We will attempt this, after first noting the following important qualifications.

When a second crack is introduced into the body, the problem becomes much more complicated. As discussed earlier, the role of crack interaction between two three-dimensional cracks, one of which is non-planar and whose detailed geometry is not well known, is a poorly understood problem. On the stress maps, successive points have been purposely offset to remind us that these solutions are strictly valid only for the case of a single, throughgoing joint. If we could somehow introduce a second crack in the body, yet require that this later crack not alter the stress field which arises solely from the throughgoing crack, then an examination of the stress field could provide valuable information about the geometry of the later crack. The degree to which this assumption violates reality is unknown, yet adoption of the assumption may allow the use of this simple analysis as a first order approximation to the much more complex multiple-crack problem.

I. *Closed crack*

For $\sigma_3^\infty = -1$ (unit tension), σ_1^∞ vertical, and an angle between σ_2^∞ and the Z-axis of 30°, the crack will be closed if $\sigma_{yy}^\infty > 0$. For the geometry specified, the condition that $\sigma_{yy}^\infty > 0$ requires that $\sigma_2^\infty > 3$. In examples I.A and I.B, σ_2^∞ has been assigned an arbitrary value of 5. Variations in the shear stress ratio on the crack, (S), lead to variations in the stress field about the crack. Solution for the stresses follows from equations (5) and (14)–(21).

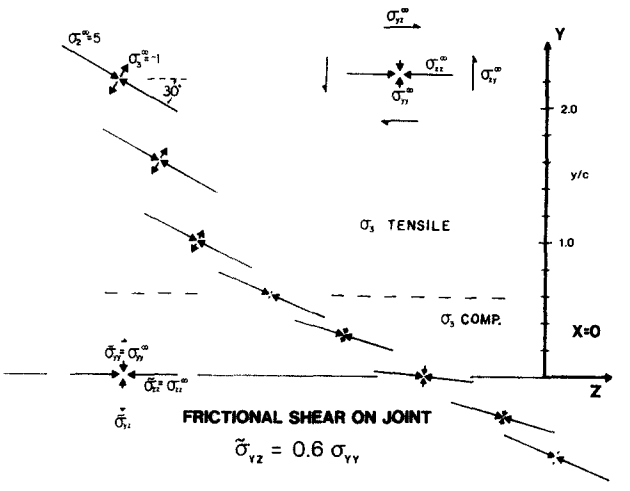

Fig. 9. Map of principal stresses about a joint subject to friction across the joint. Far-field stresses are $\sigma_2^\infty/\sigma_3^\infty = -5, \zeta = 30°$. Resolved far-field stresses are shown in the upper right. Boundary conditions on the crack are shown in the lower left. A Byerlee-type friction law is used to specify shear stress (σ_{yz}) on the joint. Note that σ_3 changes sign at $y/c \approx 0.6$. See text for details.

I.A. *Frictional sliding.* If the resolved normal stress on the joint, σ_{yy}^∞, is compressive, then the joint is closed. If the joint is not completely locked, it is possible that some frictional sliding relationship will control the shear stresses on the joint face. Byerlee (1977) found that rock type has little or no effect on friction, and that for normal stresses up to 2 kb the shear stress required to cause sliding is given approximately by:

$$\tau = 0.85\sigma_n.$$

Byerlee noted that at low stresses there is a wide variation in rock friction, and he attributed this to variation in surface roughness.

Zoned joints in the Moab Member are near-planar features that display negligible surface relief. For this reason a slightly lower coefficient of friction has been assumed. Figure 9 is the stress map resulting from use of the frictional relation

$$\sigma_{yz} = 0.6\sigma_{yy}^\infty \text{ (at } y = 0; \quad |x| < c)$$

as the boundary condition on the joint face. Using this relationship, with $\sigma_2^\infty = 5$ and $\sigma_3^\infty = -1$, the full boundary conditions are given by equations (14)–(16), with $S = 0.12$ for the far-field stress state illustrated. The solution is obtained from equation (21) with the magnitude and orientation of the perturbed principal stresses determined from a standard Mohr circle construction.

The perturbed principal stresses undergo a counterclockwise rotation in orientation. Additionally, at $y/c \approx 0.6$, the minimum principal stress, σ_3, undergoes a sign change, switching from a tensile stress for $y/c > 0.6$ to a compressive stress for $y/c < 0.6$. From $y/c = \infty$ to $y/c = 0.6$, the principal stresses undergo a counterclockwise rotation of 8°.

I.B. *Frictionless joint.* If we use the same far-field stress as in the previous example, but let the joint be

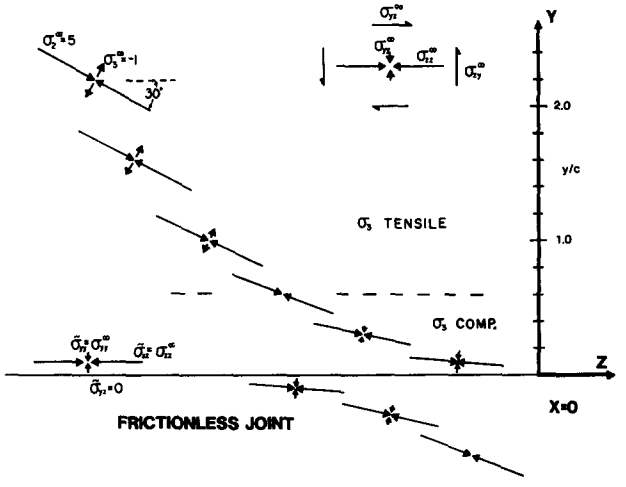

Fig. 10. Map of principal stresses about a frictionless joint under far-field stresses of $\sigma_2^\infty/\sigma_3^\infty = -5$; $\zeta = 30°$. Resolved far-field stresses are shown in the upper right. The joint ($y/c = 0$) is shear stress free (for $y = 0$; $|x| < c$, $\sigma_{yz} = 0$). Note change in sign of σ_3 at $y/c \approx 0.6$.

totally lubricated, we obtain the stress map shown in Fig. 10. The boundary conditions for this problem are given by equations (14)–(16) with $S = 0$. The solution follows that of the previous two examples.

From Fig. 10 we see that a counterclockwise rotation of the principal stresses occurs as we approach the throughgoing joint. As in the frictional sliding case, the minimum principal stress, σ_3, undergoes a sign change from tensile to compressive at $y/c \approx 0.6$.

Propagation of a younger joint. A question of considerable practical interest is whether we can predict the trace of a joint which nucleates far from the throughgoing joint of Figs. 9 or 10 and propagates toward it. How might the local perturbation of the stress field, due to the presence of the throughgoing joint, affect the orientation and propagation of the growing joint?

A basic tenet of linear elastic fracture mechanics is that the magnitude of stresses near a crack tip are proportional to the stress intensity factors (K_i, where i = I, II, III denotes, respectively, the opening, sliding and tearing modes of crack displacement) (Broek 1978, pp. 8–17). For a three-dimensional (elliptical) crack, K_i is a function of position on the crack front, the crack geometry and the loading conditions (Broek 1978, pp. 80–86). Growth of an individual crack is expected to occur when K_i somewhere on the crack front reaches a critical value which is a material property; the fracture toughness (K_i^C). There is abundant field evidence in Arches to support the contention that the zoned joints in the Moab Member originally propagated as extensional, or Mode I (opening mode) fractures. This in turn indicates that critical parameters needed to predict crack behavior include an evaluation of K_I along the crack front, and a measurement of the fracture toughness, K_I^C, of the Moab Member.

Although extensive compilations of basic solutions of stress intensity factors exist for various simple crack geometries and loading conditions (e.g. Paris & Sih 1965, Appendix II), a general solution which considers multiple (interacting) non-planar three-dimensional cracks of arbitrary shape subjected to generalized loading conditions is probably not analytically feasible. Numerical solutions for particular configurations may be tractable, but their applicability would be clouded by the uncertainty of the geometry of the crack front. Even the excellent exposures in Arches give little information regarding the exact geometry of crack fronts.

The failure criterion of linear elastic fracture mechanics (fracture propagation when $K_I = K_I^C$) is simple, elegant and apparently physically sound. However, direct application of this simple propagation criterion to the problem of interest invokes enormous complications.

Intuitively, we might expect the tip of the growing crack to cease propagating when it passes from a region of tensile stress normal to the crack front into a region of compressive stress normal to the crack front. In the Moab Member, assuming the loading conditions of either Figs. 9 or 10, this change of sign in σ_3 would occur at a distance of about 7 m from the throughgoing joint zone. The shortcoming of intuition was convincingly demonstrated by Lachenbruch (1961, 1962), who showed that a planar crack growing perpendicular to a varying stress field can propagate a considerable distance into a zone of compressive normal stress. This is possible due to the 'lever effect' whereby normal tensile stresses near the center of the crack contribute significantly to the overall stress intensity (K_I) at the crack tip, allowing high K_I values even though the crack tip proper is subject to a normal compressive stress. Thus, although the propagating crack of Figs. 9 and 10 will propagate some distance into the zone of compressive σ_3, it is not currently possible to predict exactly how far it should grow into this compressive zone because of our inability to specify a K_I value for the crack front. Nevertheless, growth of the second crack (J_2) will be retarded within the compressive zone.

For $\sigma_3^\infty = -1$ and $\zeta = 30°$, as σ_2^∞ increases, the magnitude of the retarding compressive stress within the compressive zone will increase, and the size of the compressive zone itself will increase. Thus, for $\sigma_2^\infty \gg |\sigma_3^\infty|$, we might expect the propagating joint (J_2 of Fig. 11) to grow only a small distance into the compressive zone. This is clearly in disagreement with the Arches observations that in Domain A the later generation joints parallel the throughgoing set some tens of centimeters distant from the throughgoing set (J_1). In spite of the assumptions inherent in the stress field solution, we can rule out relatively large compressive normal stresses across the throughgoing (J_1) zones during the J_2 jointing episode.

For the boundary conditions illustrated in Figs. 9 and 10, the situation is less clearcut. Although the younger joint, J_2, will grow some distance into the compressive zone, it seems doubtful that the crack will be able to extend itself by a length of more than 1.5 c, which would be required to duplicate the sigmoidal curving-parallel geometry observed in Domain A.

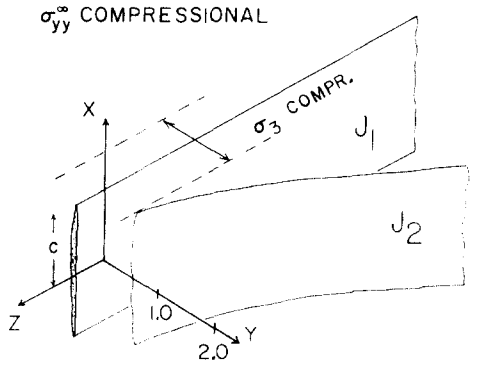

Fig. 11. Inferred resultant geometry of a younger joint zone (J_2) growing toward a throughgoing zone (J_1) for the case of σ^{∞}_{yy} compressive. A zone will exist around J_1 in which σ_3 becomes compressive. Growth of J_2 will be retarded as it encounters this zone due to the absence of tensile stresses at the crack tip. For a Byerlee-type friction law on J_1, σ_3 switches from tensile to compressive at $y/c \approx 0.6$. The maximum change in orientation of J_2 at the compressive zone boundary will be about 8° from its far-field orientation.

Two lines of field evidence suggest that J_1 zones were open cracks or fissures during the J_2 jointing episode, and thus could not have transmitted normal compressive stresses across the J_1 zones. They are: (1) a total absence of slickensides; and (2) the presence of banded mineral staining adjacent to J_1 joints. Neither line of evidence is conclusive. It is not clear that low compressive normal stresses across J_1 joints would result in slickenside features, given the small displacements documented on J_1 joints. Similarly, even if the banded mineral staining reflects fluid flow in an open J_1 joint, there is no guarantee that mineralization was synchronous with the J_2 jointing event.

The lack of slickensides, the banded mineral staining and the apparent absence of a 'compressive region' near J_1 zones, when taken together, suggest that J_1 zones were effectively free surfaces during the J_2 jointing episode. In order for J_1 joint walls to be physically separated, the far-field normal stress applied to the J_1 joints must have been tensile.

II. *Open crack*

If the resolved normal stress on the joint, σ^{∞}_{yy}, is tensile, then the joint is open and is a free surface. For $\sigma^{\infty}_3 = -1$, σ^{∞}_1 vertical and an angle of 30° between σ^{∞}_2 and the Z-axis, σ^{∞}_{yy} will be tensile for the range $-1 < \sigma^{\infty}_2 < 3$. The boundary conditions for this situation are specified in equations (7) and (8). An additional distinction can be made based on the magnitude of σ^{∞}_{zz}. For the specified geometry, σ^{∞}_{zz} will be compressive if $\sigma^{\infty}_2 > 1/3$. Over the range $-1 < \sigma^{\infty}_2 < 1/3$, σ^{∞}_{zz} will be tensile. Solutions for the local stresses are by equations (9)–(12). The principal stresses and their orientations are found from standard techniques. On the joint surface, we require that the principal stresses be perpendicular and parallel to the surface. This requires a rotation of the principal stresses, which can be accomplished by either a clockwise or counterclockwise rotation. The direction of rotation of the principal stresses is controlled by the magnitude of σ^{∞}_{zz}.

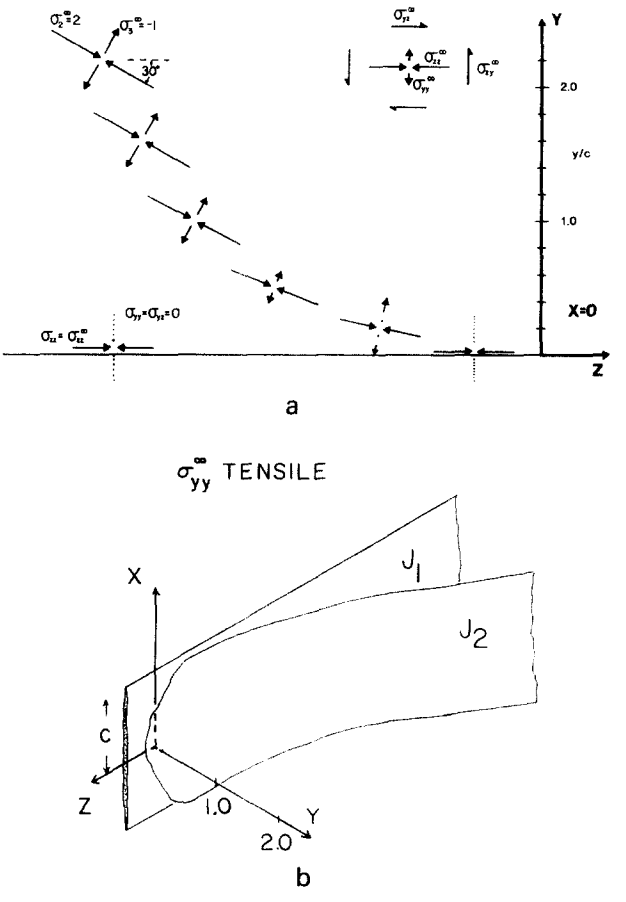

Fig. 12. (a) Map of principal stresses about a joint when the resolved far-field stress normal to the joint, σ^{∞}_{yy}, is tensile. The joint is subject to the far-field stresses $\sigma^{\infty}_2/\sigma^{\infty}_3 = -2$, with $\zeta = 30°$. Since the joint is open, $\sigma_{yy} = \sigma_{yz} = 0$ on the joint surface. Note that σ_3 remains tensile for all $y/c > 0$. As $y/c \to 0$, the principal stresses rotate such that they become parallel and perpendicular to the free surface. (b) Inferred resultant geometry of a younger joint zone (J_2) growing toward a throughgoing zone (J_1) when the resolved far-field stress normal to J_1 (σ^{∞}_{yy}) is tensile. J_1 will be a free surface. J_2 may grow arbitrarily close to, and subparallel with J_1. Compare with Fig. 2(b).

II.A. σ^{∞}_{zz} *is compressive.* If the resolved stress parallel to the joint, σ^{∞}_{zz}, is compressive, then the rotation will be counterclockwise, as shown in Fig. 12(a). A pertinent feature of this solution is that the minimum principal stress, σ_3, remains tensile for all $y > 0$.

Ignoring crack interaction, we might expect that a joint originating a distance from the throughgoing zone and propagating toward it would systematically curve in response to the rotation of the minimum principal stress, as in Fig. 12(b). In addition, for all $y > 0$ there is a tensile σ_3 available to provide a driving force for crack growth. In this manner, it might be possible for a younger joint to grow arbitrarily close to a throughgoing zone with the younger joint systematically changing its orientation until it parallels the throughgoing zone, resulting in a curving-parallel geometry. Note that the sigmoidal form could be achieved without the younger joint undergoing a shear strain anywhere along its length. Thus, a curved fracture trace need not be an indicator of a shearing mode of crack growth, as suggested by Beach (1980).

The stress map of Fig. 12(a) and the hypothetical joint trace of Fig. 12(b) bear a striking resemblance to the

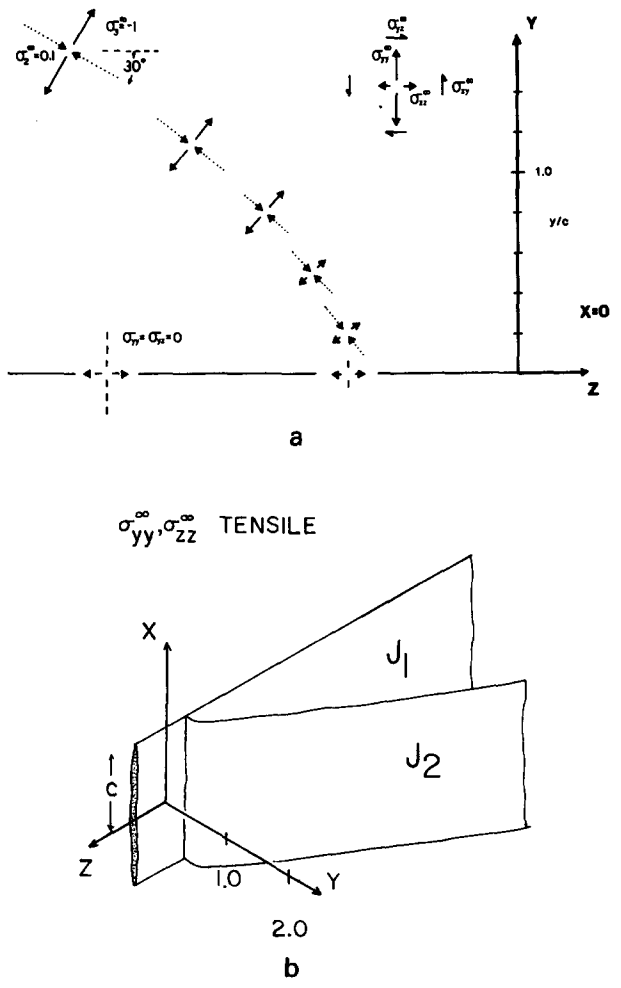

Fig. 13. (a) Map of principal stresses about a joint zone under the far-field loading $\sigma_2^\infty/\sigma_3^\infty = -0.3$; for $\zeta = 30°$. Since the resolved far-field stress normal to the zone (σ_{yy}^∞) is tensile, the joint will be an open crack and hence a free surface. Additionally, σ_{zz}^∞ is tensile, causing a clockwise rotation of the principal stresses as $y \to 0$. σ_3 will be tensile everywhere. Note the abrupt change in orientation of the principal stresses at $y/c \approx 0.2$. (b) Inferred resultant geometry of a younger joint zone (J_2) growing toward a throughgoing zone (J_1) when the resolved far-field stresses σ_{yy}^∞ and σ_{zz}^∞ are both tensile. If the propagation path of J_2 is controlled by the stress field about J_1, it will abruptly curve into J_1, at a characteristic distance of $y/c \approx 0.2$.

geometries observed on the younger joint zones in Domain A (compare with Fig. 2b). This suggests that the systematic geometries noted on J_2^A are indicative of growth of this joint set in a regional stress field in which $-3 < \sigma_2^\infty/\sigma_3^\infty < -1/3$. This estimate is strictly valid only for those J_2^A which, far from J_1^A, show a dihedral angle of 30° with J_1^A.

II.B. *σ_{yy}^∞ and σ_{zz}^∞ are both tensile.* If the joint is open, but σ_{zz}^∞ is tensile, then the situation illustrated in Fig. 13(a) is applicable. A clockwise rotation of the perturbed principal stresses will occur. The rotation is most pronounced closest to the joint. σ_3 is everywhere tensile.

Again ignoring crack interaction, we might expect a joint originating far away and growing toward the throughgoing zone to curve abruptly into the older zone (Fig. 13b). The sudden change in curvature would occur at $y/c \approx 0.2$. For the Moab Member, the characteristic distance at which the curvature would be expected to abruptly change is about 2.7 m. This is in excellent agreement with the observations in Domain B (compare with Fig. 3b).

The similarities between the curving-perpendicular geometries of J_2^B joints and the hypothetical joint trace of Fig. 13(b) suggest that J_2^B grew in a regional stress field in which $-1/3 < \sigma_2^\infty/\sigma_3^\infty < 1$. This assumes that J_2^B makes a far-field dihedral angle of 30° with J_1^B.

CONCLUSIONS

Several generations of zoned joints are developed in the Moab Member of the Entrada Sandstone in Arches National Park, Utah. The sets of zoned joints are paleostress indicators. Although a joint zone originates in response to a tensile driving stress ($\sigma_3 - P < 0$), later rotation of the far-field principal stresses leads to a resolved shear parallel to the plane of the crack. Younger joints growing in the rotated stress field may display a systematic change in their orientation near an older, throughgoing zone. The interactive geometries observed are due to local rotation of principal stresses near a pre-existing, throughgoing joint zone. Characteristic interactions between different generations of zoned joints may be used to infer the ratio of the far-field horizontal principal stresses during an episode of joint growth. Different domains of joint interactions characterize areas in which the the ratio of far-field principal horizontal stresses is essentially constant.

Acknowledgements—This work is part of a Ph.D. dissertation conducted at Stanford University. The guidance of Professors Amos Nur and David Pollard are gratefully acknowledged. Funding for this study was provided by the industrial consortium sponsors of the Stanford Rock Physics Project. The co-operation and field support provided by Arches National Park and the Canyonlands National History Association merit special recognition. Reviews by Terry Engelder and an anonymous reviewer greatly improved the manuscript.

REFERENCES

Baars, D. L. & Stevenson, G. M. 1981. Tectonic evolution of the Paradox Basin, Utah and Colorado. In: *Geology of the Paradox Basin* (edited by Wiegand, D. L.). Rocky Mtn. Assoc. Geol. Field Conf. Guidebook, 23–31.

Beach, A. 1980. Numerical models of hydraulic fracturing and the interpretation of syntectonic veins. *J. Struct. Geol.* **2**, 425–438.

Bergkvist, H. & Guex, L. 1979. Curved crack propagation. *Int. J. Fract.* **15**, 429–441.

Birch, F. 1966. Compressibility; elastic constants. In: *Handbook of Physical Constants* (edited by Clark, S. P.). *Mem. geol. Soc. Am.* **97**, 97–173.

Broek, D. 1978. *Elementary Engineering Fracture Mechanics*. Sijthoff and Noordhoff, The Netherlands.

Byerlee, J. 1977. Friction of rocks. In: *Proc. Conf.* II: *Experimental Studies of Rock Friction with Application to Earthquake Prediction* (edited by Evernden, J. F.). U.S. Geol. Surv., 55–79.

Cater, F. W. 1970. Geology of the Salt Anticline region in southwestern Colorado. *U.S. Geol. Surv. Prof. Paper* 637.

Dane, C. H. 1935. Geology of the Salt Valley Anticline and adjacent areas, Grand County, Utah. *Bull. U.S. geol. Surv.* 863.

Doelling, H. H. 1985. Geologic map of Arches National Park and vicinity, Grand County, Utah. *Utah Geol. Mineral Survey Map* 74 and accompanying text.

Durney, D. W. & Ramsay, J. G. 1973. Incremental strains measured by syntectonic crystal growths. In: *Gravity and Tectonics* (edited by DeJong, K. & Schoten, R.). Wiley Interscience, New York, 67–96.
Dyer, J. R. 1979. A 3-D elastic bending-plate model for joint formation. *EOS* **60**, 944.
Dyer, J. R. 1983. Jointing in sandstones, Arches National Park, Utah. Unpublished PhD. dissertation, Stanford University.
Eftis, J. & Leibowitz, H. 1972. On the modified Westergaard equations for certain plane crack problems. *Int. J. Fracture Mech.* **8**, 383–392.
Eftis, J., Subramonian, N. & Leibowitz, H. 1977. Crack border stress and displacement equations revisited. *Engng Fract. Mech.* **9**, 189–210.
Engelder, T. & Geiser, P. 1980. On the use of regional joint sets as trajectories of paleostress fields during the development of the Appalachian Plateau, New York. *J. geophys. Res.* **85**, 6319–6341.
Eshelby, J. D. 1968. Stress analysis. In: *Fracture Toughness.* ISI Publication 121, The Iron and Steel Institute, London, 13–48.
Griggs, D. & Handin, J. 1960. Observations on fracture and a hypothesis of earthquakes. In: *Rock Deformation (A Symposium)* (edited by Griggs, D. & Handin, J.). *Mem. geol. Soc. Am.* **79**, 347–364.
Hodgson, R. A. 1961. Classification of structures on joint surfaces. *Am. J. Sci.* **259**, 493–502.
Hoek, E. & Bieniawski, Z. T. 1965. Brittle fracture propagation in rock under compression. *Int. J. Fracture Mech.* **1**, 137–155.
Hubbert, M. K. & Willis, D. G. 1957. Mechanics of hydraulic fracturing. *Trans. Am. Inst. Min. Metall. Petrol. Engrs* **210**, 153–166.
Kehle, R. O. 1964. The determination of tectonic stresses through analysis of hydraulic well fracturing. *J. geophys. Res.* **69**, 259–273.
Kulander, B. R., Barton, C. C. & Dean, S. L. 1979. The application of fractography to core and outcrop fracture investigations. *U.S. Dept of Energy*, Publication METC/SP-79/3.
Lachenbruch, A. H. 1961. Depth and spacing of tension cracks. *J. geophys. Res.* **66**, 4273–4292.
Lachenbruch, A. H. 1962. Mechanics of thermal contraction cracks and ice-wedge polygons in permafrost. *Spec. Pap. geol. Soc. Am.* **70**.
Odé, H. 1957. Mechanical analysis of the dike pattern of the Spanish Peaks area, Colorado. *Bull. geol. Soc. Am.* **68**, 567–576.
O'Sullivan, R. B. 1981. Stratigraphic sections of Middle Jurassic Entrada Sandstone and related rocks from Salt Valley to Dewey Bridge in East-Central Utah. *U.S. geol. Surv. Oil and Gas Investigations Chart* OC-113.
Paris, P. C. & Sih, G. C. 1965. Stress analysis of cracks. In: *Fracture Toughness and Testing.* ASTM Special Technical Publication No. 381; Soc. for Testing Materials, Philadelphia, Pennsylvania, 30–81.
Peng, S. S. & Ortiz, C. A. 1973. Crack propagation and fracture of rock specimens loaded in compression. In: *Dynamic Crack Propagation* (edited by Sih, G. C.). Sijthoff and Noordhoff, The Netherlands, 113–129.
Pollard, D. D. & Holzhausen, G. 1979. On the mechanical interaction between a fluid-filled fracture and the earth's surface. *Tectonophysics* **53**, 27–57.
Ramsay, J. G. 1967. *Folding and Fracturing of Rocks.* McGraw-Hill, New York.
Ramsay, J. G. & Graham, R. H. 1970. Strain variation in shear belts. *Can. J. Earth Sci.* **7**, 786–813.
Roering, C. 1968. The geometrical significance of natural en echelon crack-arrays. *Tectonophysics* **5**, 107–123.
Secor, D. T. 1965. Role of fluid pressure in jointing. *Am. J. Sci.* **263**, 633–646.
Secor, D. T. 1969. Mechanism of natural extension fracturing at depth in the earth's crust. *Geol. Surv. Canada Paper* 68-52, 3–47.
Segall, P. & Pollard, D. D. 1980. Mechanisms of discontinuous faults. *J. geophys. Res.* **85**, 4337–4350.
Shainin, V. E. 1950. Conjugate sets of en echelon tension fractures in the Athens Limestone at Riverton, Virginia. *Bull. geol. Soc. Am.* **61**, 509–517.
Sih, G. C. 1966. On the Westergaard method of crack analysis. *Int. J. Fracture Mech.* **2**, 628–631.
Westergaard, H. M. 1939. Bearing pressures and cracks. *J. Appl. Mech.* **61**, A49–A53.
Wheeler, R. L. & Holland, S. M. 1981. Style elements of systematic joints: an analytic procedure with a field example. In: *Proceedings of the Third International Conference on Basement Tectonics* (edited by O'Leary, D. W. & Earle, J. L.), 393–404.
Williams, P. L. 1964. Geology, structure, and uranium deposits of the Moab quadrangle, Colorado and Utah. *U.S. geol. Surv. Misc. Inv. Map* I-360.
Zoback, M. D. & Pollard, D. D. 1978. Hydraulic fracture propagation and the interpretation of pressure-time records for *in situ* stress determinations. *19th U.S. Symposium on Rock Mechanics*, 14–22.

APPENDIX

The approximation of a single zone of joints as a simple, infinitely long crack with a characteristic height allows a relatively straightforward analytic solution of the elastic stress fields about the crack. Because of the simple geometry and assumptions made about the loading, we can obtain a solution to the three-dimensional problem as a linear superposition of the solutions to two separate, well-known two-dimensional problems from linear elastic fracture mechanics: the plane (Mode I loading) and antiplane (Mode III loading) problems. The treatment follows the standard methodology, differing only in that the entire solution is utilized, not just the crack tip approximation.

The solutions are based on the complex potential method of Westergaard (1939), which is treated lucidly in Appendix I of Paris & Sih (1965). Limitations of Westergaard's solutions are discussed by Sih (1966), Eftis & Liebowitz (1972) and Eftis *et al.* (1977).

We assume infinitesimal linear elasticity in an infinite, isotropic homogeneous body. Body forces are not considered. The crack geometry and co-ordinate system are shown in Fig. 14. One of the far-field principal stresses, σ_1^∞ or σ_2^∞, is colinear with the X-axis. Based on field evidence, we assume throughout that σ_1^∞ is vertical and colinear with the X-axis.

Mode I problem

When the far-field normal stress on the crack face (σ_{yy}^∞) is tensile, as in Fig. 8, the Mode I (opening mode) solution of linear elastic fracture mechanics is applicable. If a uniform internal pressure within the crack, P_i, is considered, then the Mode I solution is applicable if ($\sigma_{yy}^\infty - P_i$) < 0. An example of the straightforward application of this solution is solving for the stress field around an igneous dike intruding into drained rocks. For the plane, two-dimensional crack in the X–Y plane subjected to biaxial loading, we must satisfy the equilibrium equations:

$$\frac{\partial \sigma_{xx}}{\partial x} + \frac{\partial \sigma_{xy}}{\partial y} = 0$$

$$\frac{\partial \sigma_{xy}}{\partial x} + \frac{\partial \sigma_{yy}}{\partial y} = 0$$

$$\sigma_{xy} = \sigma_{yx}, \qquad \text{(A1)}$$

while the strain–displacement relations and Hooke's law lead to the compatibility equation

$$\left(\frac{\partial^2}{\partial x^2} + \frac{\partial^2}{\partial y^2}\right)(\sigma_{xx} + \sigma_{yy}) = 0. \qquad \text{(A2)}$$

If a uniform internal pressure within the crack, P_i, is considered,

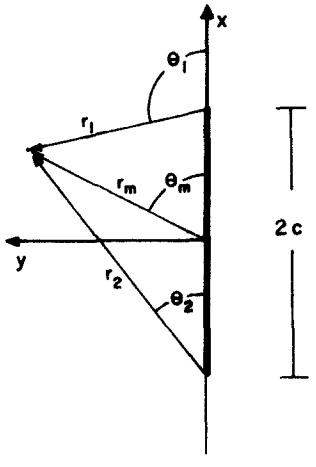

Fig. 14. Co-ordinate system used for the full solution of the elastic stress field about a plane flat elliptical crack.

then the boundary conditions to be satisfied are:

$$\begin{aligned} &\text{for } y = 0,\ |x| < c: && \sigma_{yy} = P_i \\ &&& \sigma_{xy} = 0 \\ &\text{for } (x^2 + y^2)^{1/2} \to \infty: && \sigma_{yy} = \sigma^{\infty}_{yy} \\ &&& \sigma_{xx} = \sigma^{\infty}_{xx}. \end{aligned} \tag{A3}$$

It is convenient to use the co-ordinate system defined in Fig. 14. The general solution to the plane, uniform biaxial loading problem of Fig. 8(b) can be derived using the methodology of Paris & Sih (1965, Appendix I). The full solutions are:

$$\sigma_{xx} = (\sigma^{\infty}_{yy} - P_i)\left[\frac{r_m}{(r_1 r_2)^{1/2}} \cos\left(\theta_m - \frac{\theta_1 + \theta_2}{2}\right) - \frac{|y|c^2}{(r_1 r_2)^{3/2}} \sin\left(\tfrac{3}{2}(\theta_1 + \theta_2)\right)\right] + \sigma^{\infty}_{xx} - (\sigma^{\infty}_{yy} - P_i) \tag{A4}$$

$$\sigma_{yy} = (\sigma^{\infty}_{yy} - P_i)\left[\frac{r_m}{(r_1 r_2)^{1/2}} \cos\left(\theta_m - \frac{\theta_1 + \theta_2}{2}\right) + \frac{|y|c^2}{(r_1 r_2)^{3/2}} \sin\left(\tfrac{3}{2}(\theta_1 + \theta_2)\right)\right] + P_i \tag{A5}$$

$$\sigma_{xy} = (\sigma^{\infty}_{yy} - P_i)\left[\frac{yc^2}{(r_1 r_2)^{3/2}} \cos\left(\tfrac{3}{2}(\theta_1 + \theta_2)\right)\right] \tag{A6}$$

$$\sigma^{I}_{zz} = \nu[\sigma_{xx} + \sigma_{yy}]. \tag{A7}$$

In general, σ_{xy} shearing stresses will increase near the crack tips, leading to a local rotation of principal stresses about the Z-axis. If we limit our investigation to the plane $x = 0$, then:

$$\begin{aligned} \theta_m &= \frac{\pi}{2} \\ \theta_1 + \theta_2 &= \pi \\ r_m &= y \\ r_1 = r_2 &= (y^2 + c^2)^{1/2}; \end{aligned} \tag{A8}$$

and equations (A4)–(A6) become:

$$\sigma_{xx}(x = 0) = (\sigma^{\infty}_{yy} - P_i)\left[\frac{|y|}{(y^2 + c^2)^{1/2}}\left(1 + \frac{c^2}{y^2 + c^2}\right)\right] + \sigma^{\infty}_{xx} - (\sigma^{\infty}_{yy} - P_i) \tag{A9}$$

$$\sigma_{yy}(x = 0) = (\sigma^{\infty}_{yy} - P_i)\left[\frac{|y|}{(y^2 + c^2)^{1/2}}\left(1 - \frac{c^2}{y^2 + c^2}\right)\right] + P_i, \tag{A10}$$

and

$$\sigma_{xy}(x = 0) = 0. \tag{A11}$$

For $\sigma_{xy} = 0$, there will be no principal stress rotations about the Z-axis due to the Mode I part of the solution.

Mode III problem

The problem shown in Fig. 8(d) corresponds to the antiplane strain (Mode III loading) problem of linear elastic fracture mechanics. In this problem, an infinitely long crack with characteristic height $2c$ is subjected to a far-field antiplane pure shear of magnitude $(1 - S)\sigma^{\infty}_{yz}$, where S is defined by equation (17). We require that the crack face be traction-free. If u, v, w are displacements in the X, Y and Z directions, respectively, then the Mode III problem is specified by:

$$u = 0; \quad v = 0; \quad w = w(x, y). \tag{A12}$$

Since this is a case of pure shear,

$$\sigma^{d}_{xx} = \sigma^{d}_{yy} = \sigma^{d}_{zz} = \sigma^{d}_{xy} = 0, \tag{A13}$$

where the superscript d refers to Fig. 8(d).

The equilibrium equations become

$$\frac{\partial \sigma^{d}_{xz}}{\partial x} + \frac{\partial \sigma^{d}_{xz}}{\partial y} = 0, \tag{A14}$$

while the strain–displacement relations and Hooke's law give

$$\varepsilon^{d}_{xz} = \frac{\partial \omega}{\partial x} = \frac{\sigma^{d}_{xz}}{G}$$

$$\varepsilon^{d}_{yz} = \frac{\partial \omega}{\partial y} = \frac{\partial^{d}_{yz}}{G}, \tag{A15}$$

where G is the shear modulus. The boundary conditions for the Mode III problem are:

$$\begin{aligned} &\text{at } y = 0,\ |x| < c; && \sigma^{d}_{yz} = \sigma^{d}_{xz} = 0, \\ &\text{at } (x^2 + y^2)^{1/2} \to \infty; && \sigma^{d}_{yz} = (1 - S)\sigma^{\infty}_{yz}. \end{aligned} \tag{A16}$$

Using the co-ordinate system defined in Fig. 14, the solution is given by Eshelby (1968, equation 20) as:

$$\sigma^{d}_{yz} = (1 - S)\left[\sigma^{\infty}_{yz} \frac{r}{(r_1 r_2)^{1/2}} \cos\left(\theta - \frac{\theta_1 + \theta_2}{2}\right)\right], \tag{A17}$$

$$\sigma^{d}_{xz} = (1 - S)\left[\sigma^{\infty}_{yz} \frac{r}{(r_1 r_2)^{1/2}} \sin\left(\theta - \frac{\theta_1 + \theta_2}{2}\right)\right]. \tag{A18}$$

On the plane $x = 0$, using the relations of (A8), we find that

$$\sigma^{d}_{yz}(x = 0) = (1 - S)\left[\sigma^{\infty}_{yz} \frac{y}{(y^2 + c^2)^{1/2}}\right], \tag{A19}$$

$$\sigma^{d}_{xz}(x = 0) = 0. \tag{A20}$$

Non-zero σ_{yz} and σ_{xz} shearing stresses will cause rotation of the principal stresses about the X- and Y-axes, respectively. On the plane $x = 0$, the only non-zero shear stress is σ_{yz}. This will lead to a rotation of the principal stress axes about the X-axis.